COIN-GPS: Indoor Localization from Direct GPS Receiving

Shahriar Nirjon[1], Jie Liu[2], Gerald DeJean[2], Bodhi Priyantha[2], Yuzhe Jin[2], Ted Hart[2]
[1] Department of Computer Science, University of Virginia
[2] Microsoft Research, Redmond, WA
smn8z@virginia.edu, {liuj, bodhip, dejean, yuzjin, tedhar}@microsoft.com

ABSTRACT

Due to poor signal strength, multipath effects, and limited on-device computation power, common GPS receivers do not work indoors. This work addresses these challenges by using a steerable, high-gain directional antenna as the front-end of a GPS receiver along with a robust signal processing step and a novel location estimation technique to achieve direct GPS-based indoor localization. By leveraging the computing power of the cloud, we accommodate longer signals for acquisition, and remove the requirement of decoding timestamps or ephemeris data from GPS signals. We have tested our system in 31 randomly chosen spots inside five single-story, indoor environments such as stores, warehouses and shopping centers. Our experiments show that the system is capable of obtaining location fixes from 20 of these spots with a median error of less than 10 m, where all normal GPS receivers fail.

Keywords

Indoor GPS, Instant GPS, CO-GPS, COIN-GPS

1. INTRODUCTION

Common wisdom believes that GPS receivers do not work indoors, period. GPS signals are extremely weak when they reach the Earth's surface, and further attenuation and multipath effects caused by the building shell make satellites undetectable. In fact, we have all experienced a frozen 'acquiring satellites' screen or the 'lost satellite reception' message on a GPS receiver when the device is inside a building or when the line-of-sight between the receiver and the satellites is obstructed. This paper presents a method of using GPS-based direct localization in some indoor environments.

Indoor localization and location-based services have gained great attention recently while people have enjoyed their outdoor counterparts for years. Indoor navigation in shopping malls, indoor location-based advertisements, and tracking friends and family members in indoor public places are a few examples of how indoor location information can make services friendlier and more useful. Because common GPS receivers do not work indoors due to low GPS signal strength and multipath effects, indoor location systems are usually much more complicated than direct GPS receiving. Existing indoor localization approaches are either based on signature matching or continuous tracking.

There are many kinds of signatures that can approximately associate a receiver with an indoor location. Some examples include, RF signatures like WiFi [7], FM [10], cellular networks, Bluetooth beacons, magnetic signatures from either the Earth's magnetic field [12] or deployed beacons [18], ambient sound signatures [6], and cameras [23, 31]. The challenges of all these approaches are infrastructure setup and profiling. The accuracy of most signature-based approaches directly relates to the density of signal sources. At the same time, the indoor space must be profiled (in many cases repeatedly to accommodate temporal variations) to map signatures to location coordinates. A second class of localization approaches is based on continuously tracking the movement of the target from a known location [39, 29]. However, motion sensing based on accelerometer, compass, and gyro drifts over time. The methods must rely again on signatures to realign tracking processes. Continuous sensing and processing also challenge the battery lives of mobile devices.

In contrast to the above approaches, GPS receiving, when working effectively, is direct. A device does not need to have prior knowledge of a known location to start with. Each location can be computed independently, and there is no additional infrastructure or profiling necessary. Our goal is to extend GPS receiving to indoor environments, where it can either be used directly by consumer devices, or be used in conjunction with profiling and tracking methods as landmarks.

Building an indoor GPS receiver is challenging for several practical reasons. First, signals from the GPS satellites are inherently weak, and after traveling more than 21000 km to reach the Earth's surface, the signal strength (-125 dBm) is barely enough to decode satellite information outdoors. Note that the thermo-noise floor at GPS frequency is about -111 dBm. Indoors, the signal-strength is about 10 to 100 times weaker, and it is almost impossible for a typical GPS receiver to acquire any satellite. Second, even if signals from a satellite are detected indoors, the weaker signal strength combined with increased multipath effects can cause the receiver to compute an inaccurate distance from

the satellite and yield an estimated location that is miles away from the true location. Third, location estimation in a typical GPS receiver requires at least 4 visible satellites, which is highly unlikely to be obtained in an indoor environment. In this paper, we address these challenges and propose a high-sensitivity cloud-offloaded instant GPS (COIN-GPS) for indoors.

We take a hardware-software approach in COIN-GPS, in which, a high-gain directional antenna is used at the front-end of the receiver, and the locations are computed in the cloud. The design of COIN-GPS is motivated by several properties of indoor environments.

- The roof materials of a building are heterogeneous. We perform a simulation study to understand the amount of attenuation a GPS signal undergoes when it penetrates through different building materials. We conclude that, by steering a directional antenna towards different directions, it is possible to achieve a higher SNR in a certain direction than an omni-directional antenna. Directional antennas also help mitigate the multipath effects introduced by the building structure.
- Indoor GPS signals are too weak to decode any data packets for timestamps and ephemeris. By using a cloud-offload approach [22], we eliminate the need to decode any GPS data. We only store the raw signals at the intermediate frequency as necessary and rely upon the cloud for the ephemeris and location calculation.
- Indoor subjects move slowly. The receiver's location does not change much within a short period of time. By exploiting this, we are able to reuse satellites by considering the same satellite, acquired at different points in time, as different satellites. We derive the formula that, for M independent directions, a total of $2M + 3$ satellites are required to get a successful location fix in such cases.

COIN-GPS is inspired by CO-GPS, an energy efficient signal sampling and cloud-offloaded location computation paradigm [22]. However, COIN-GPS is also different in a number of major aspects. For example, the goal of CO-GPS is to save energy, whereas, COIN-GPS's aim is to achieve high sensitivity. COIN-GPS uses a custom designed, high-gain directional antenna, whereas CO-GPS uses a regular omni-directional antenna. Finally, COIN-GPS incorporates two new signal processing algorithms, one for robust satellite acquisition and another for estimating the location of a stationary receiver when the number of satellites is inadequate. Both of these algorithms are designed specifically for indoors, taking advantages of the relatively low speed of indoor movements. Like CO-GPS, COIN-GPS is suitable for delay tolerant applications where the data is collected in-situ and processed offline. But compared to 30+ s time-to-first-fix in an outdoor GPS with cold start, COIN-GPS's execution-time performance is acceptable for many indoor location-based applications too. CO-GPS is used as a baseline for comparison in our experiments.

In order to demonstrate the performance of COIN-GPS, we evaluate the system in five randomly chosen public places in the greater Bellevue, WA area: Starbucks, Home Depot, Fred Meyer, Costco, and Bellevue Square Mall. We perform a series of experiments to show that, by virtue of the directional antenna and the robust acquisition algorithm, COIN-GPS acquires at least 3 satellites more than 60% of the time, and by combining acquired satellites from 3 or more directions, COIN-GPS gets successful location fixes in 65% of the cases, with an average localization error of 17.4 m and a median error of less than 10 m. Compared to this, traditional GPS hardly ever acquires a satellite and never gets a location fix.

The main contributions of this paper are the following:

- The design and implementation of a high-gain directional antenna and a robust acquisition algorithm that is motivated by the properties of an indoor environment.
- The formulation and implementation of the stationary GPS formula which says that for M independent directions, a total of $2M + 3$ satellites are required to get a successful location fix in indoor environments.
- The design and implementation of a complete system called COIN-GPS, which is shown to work in several indoor environments with a success rate of 65% and a median localization error of 9.6 m.

The rest of the paper is organized as follows. We briefly introduce necessary GPS concepts in Section 2. In Section 3, we study RF properties of common building materials to motivate our solution. In Section 4, we give an overview of COIN-GPS, and then Sections 5, 6, and 7 drill down to the details of three key technologies in the solution. We evaluate COIN-GPS in Section 8 and provide a discussion in Section 9.

2. GPS TERMINOLOGIES

To make this paper self-contained, we briefly introduce some key GPS concepts. We refer interested readers to [24, 37] for more technical details.

GPS Satellites: There are 32 GNSS satellites in the sky, each orbiting the earth about two cycles a day. The satellites simultaneously and continuously broadcast time and orbit information through CDMA signals at 1.575 GHz towards the Earth. A GPS receiver computes its location by measuring the distance from the receiver to multiple satellites.

Code Phase: Each satellite encodes its signal using a satellite-specific coarse/acquisition (C/A) code of length 1023 chips at 1023 Mbps, i.e. repeating every millisecond. The purpose of the C/A code is to allow a receiver to identify the sending satellite and estimate the propagation delay. Typically, GPS signals take from 64 to 89 ms to travel from a satellite to the earth. To obtain an accurate distance measurement, the receiver must estimate the signal propagation delay to the microsecond level. Since C/A codes repeat every ms, one way to estimate the sub-ms part of the propaga-

tion delay is to identify the code phase, i.e. the offset of the C/A code when it was received.

Doppler Shifts: The Doppler frequency shift is caused by the motion of the satellite and by any movement of the receiver. For example, a rising GPS satellite moves at up to 800 m/s towards a receiver, causing a frequency shift of 4.2 kHz. A shift of the same magnitude occurs in the opposite direction for a setting satellite. To reliably compute a correction under this shift, the receiver must generate the C/A code within 500 Hz of the shifted frequency. Therefore, in the frequency dimension, the receiver needs to search up to 18 bins. Most GPS receivers use 25 to 40 frequency bins to provide a better receiver sensitivity.

Acquisition, Tracking, and Location Estimation: The task of getting a location fix is divided mainly into two subtasks: satellite acquisition and location estimation. Acquisition usually involves a search process, where, for each satellite, the C/A code is correlated with the received signals to check if the satellite is present or not. Once satellites are acquired, tracking is the process of progressively adjusting code phase and Doppler shifts without going through the full acquisition process again. If a satellite is present, its trajectory and a precise timestamp can be decoded from the satellite signal. From that, the distance from the satellite to the receiver, called the pseudo-range, is obtained. Depending on the type of GPS solutions, estimation of location requires pseudo-ranges from 4 to 5 acquired satellites to form a least squares optimization process. More details of these two steps are in Section 5 and Section 6, prior to the description of our own approaches to them.

Acquisition is a computationally intensive process due to the large code phase and Doppler search space. Time-To-First-Fix (TTFF) is the elapsed time between turning on a receiver and obtaining the first location fix. Depending on what prior knowledge the receiver has about the satellites, TTFF varies from 30+ seconds in standalone GPS receivers to 6+ seconds in assisted GPS (AGPS) where the satellite trajectories are provided to the receivers through a separate channel. Typical AGPS receivers still decode timestamps from satellite signals.

CO-GPS: CO-GPS stands for the Cloud Offloaded GPS. CO-GPS is an extremely low power GPS receiver for delay-tolerant applications. The core idea of CO-GPS is to log a minimal amounts of signals (1-2 ms) at runtime and process them offline. This allows the device to aggressively duty-cycle in order to increase its lifetime. CO-GPS adopts coarse time navigation (CTN) [37], in which, neither ephemeris *nor the time stamp* is decoded from the packet; rather, a coarse time reference from a nearby landmark is used to estimate the ms part of the propagation delay, and only the sub-ms part, i.e. the code phase, is computed from the packet. This results in a GPS receiver that uses as little as a 1 ms signal, and hence, the TTFF can be as fast as a few ms. Because of this, a GPS with CTN is often called an Instant GPS. Unlike standard CTN, CO-GPS leverages the computing resources in the cloud to generate a number of candidate landmarks and use other geographical constraints to filter out the wrong solutions. Since CO-GPS does not have to decode the entire data packet, it is less susceptible to errors in environments where signal strength is weak. This is a key advantage we try to leverage in COIN-GPS.

3. MOTIVATION OF COIN-GPS DESIGN

The design of COIN-GPS is motivated by observations on indoor signal attenuation and an indoor receiver's motion.

3.1 GPS Signal Attenuation Indoors

GPS signals are inherently weak from the source. The total radiated power from a GPS satellite is about 500 W (or 27 dBW). Assuming a 21000 km distance between the satellite and the receiver (the actual distance depends on the elevation angle), the free space path loss is about 182 dB. That results in a received signal strength, in ideal conditions, of −155 dBW (or −125 dBm), which is actually below the ambient RF noise floor (typically around −111 dBm). Traditional GPS receivers use a high-gain front end, precise band pass filters and, most importantly, the SNR gain from C/A code correlation to detect the existence of GPS signals.

Indoor environments bring significant challenges to GPS signal acquisition since building materials further reduce the signal strength by 10 to 100 times, yet the strength of the RF noise floor remains the same. Amplifying the signals at the GPS frequency will not be effective. Using longer, repeated C/A code may appear to be a promising approach. However, since C/A codes are used to modulate GPS data packets, without knowing the packet content in advance, the correlation operation may go across the boundaries of opposite bits, which cancels out the correlation gain. We will discuss a more robust correlation algorithm in Section 5.

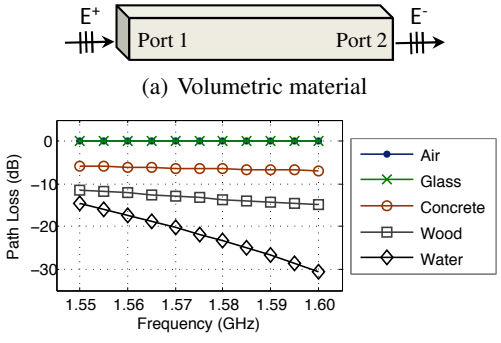

(a) Volumetric material

(b) Path Loss

Figure 1: Path loss of GPS signals through air, glass, concrete, wood, and water. Steel (not drawn) is < −200 dB.

3.1.1 A Simulation Study of GPS Signal Attenuation

To motivate our solution, we first quantify the GPS signal attenuation through different building materials. We use a simulation software called CST Microwave Studio [1] which is one of the most recognized simulators used in the RF or electromagnetic community for VHF and UHF applications.

As shown in Figure 1(a), we setup a waveguide of dimensions $6.2 \times 3.1 \times 12$ inches. These dimensions correspond to the fundamental propagating transverse electric mode (TE_{10}) of an air-filled rectangular waveguide. The materials examined in the volume are glass, concrete, wood, water, and steel. In addition, an empty waveguide (simulated as air) is evaluated as a baseline case. The GPS signal is a Gaussian wave propagating in the direction of the volume's length from the Port 1 to the Port 2, and polarized in the direction of the volume's height. We measure the ratio of received voltage signal at Port 2 to the voltage signal transmitted at Port 1, and call it the path loss.

Figure 1(b) shows the path loss versus frequency for the 6 cases considered in this study. GPS frequency is 1.575 GHz, which is in the middle of the plot. We see that the signals that propagate through air and glass are unaffected by those materials. The path loss for concrete and wood are in the range of -5 dB to -15 dB, but water and steel present significant obstructions for a GPS signal to be received. Figure 2 illustrates a 2D electric field plot of the GPS signal traveling from transmit Port 1 to receive Port 2, which gives a sense of path loss versus the thickness of the materials.

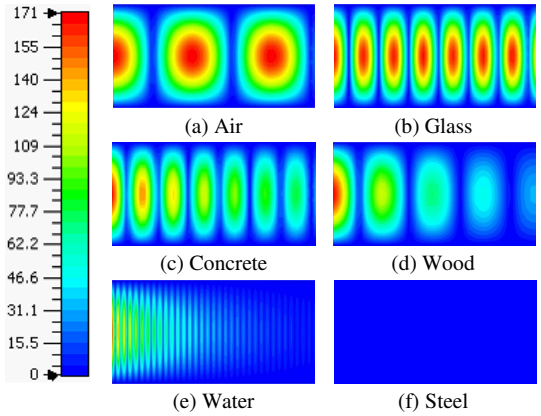

Figure 2: 2D electric field plots of a GPS signal propagating through different materials.

We have several observations through this simulation study:

- Each foot of concrete or wood attenuate the signal by $5-15$ dB. For multistory buildings, each floor will introduce this amount of path loss, which makes the problem extremely hard. So, in this paper, we will focus on single floor structures, such as shopping malls, department stores, and business parks.
- The roof of a commercial building is typically made from multiple layers of materials, such as wood, fiber glass, polymer, and asphalt. Its RF path loss property should be close to the combination of wood, glass, and concrete in the simulation. So we expect $10-20$ dB attenuation.
- Many commercial buildings have glass as part of the roof, such as skylights. They allow GPS signals to penetrate the roof with small path loss.

3.2 Motion of an Indoor Receiver

One big difference between an indoor and an outdoor GPS receiver is that the receiver moves slowly indoors. An average person walks about 3 mph, which is $10-25$ times slower than a motor vehicle's speed. Compared to the GPS satellites' pseudo-range rate of 800 m/s, practically, an indoor receiver can be assumed stationary. This motivates us to reuse satellites, i.e. to consider the same satellite, acquired at different points in time, as different reference satellites. This is a crucial assumption in COIN-GPS's location estimation algorithm, which allows us to overcome the inadequate satellites problem, which is highly likely indoors, and to estimate the location even when the number of unique satellites is less than the required minimum.

4. OVERVIEW OF COIN-GPS

Our high-sensitivity indoor GPS solution incorporates three key technologies: a directional antenna, a robust acquisition algorithm, and a multi-directional location estimation algorithm.

4.1 Directional Antenna

The simulation study and the observations in Section 3.1, motivate us to leverage a directional antenna for GPS receiving. Directional antennas selectively amplify the signals from a chosen direction. As a result, noise (and signals) from other directions are suppressed. For example, in an indoor environment, if we point the antenna towards part of the roof that introduces low signal attenuation, especially skylights, we have a greater opportunity to receive good quality GPS signals while suppressing signals from other directions. GPS satellites scatter in the sky by design. Amplifying towards one satellite may decrease the possibility of acquiring others. That's why we need to point the antenna towards different directions and carefully combine the results.

There are many antenna topologies that can be used to create a directional radiation. Some of the more popular directional antennas are Yagi-Uda arrays [34], slot antennas [14], reflector antennas [30], and patch antenna arrays [27]. Yagi-Uda arrays and reflector antennas are difficult to design in a compact form factor. Although slot antennas over a ground plane have a small form factor, they have a lower gain than desired for highly directional coverage. Patch antenna arrays present a balanced tradeoff between high gain and a compact form factor. They are also highly desirable for their ability to be independent of size and frequency by changing the dielectric material and/or utilizing compact design methods for miniaturization [20]. We discuss our implementation using a patch antenna array in Section 7.1. For now, it is suffice to assume a directional antenna that can provide ≈ 10 dB gain at the pointed direction.

4.2 Robust Acquisition

The directional antenna is used to sample and store raw GPS signals from multiple directions at the same physical

location. Each chunk of samples, obtained from a particular direction, undergoes a robust satellite acquisition process which is described in detail in Section 5. The outcome of the acquisition process is what we call a *directional acquisition*, which consists of a list of satellites, their code phases and Doppler shifts. The directional acquisition processes are run in parallel for a speedup. Once we have results from all N directions at a particular location, those having fewer than 2 acquired satellites are discarded, and the rest are merged to form a combined acquisition result having M ($M \leq N$) directional acquisitions.

The reason a directional acquisition having < 2 satellites is useless is because each time we combine acquired satellites from a certain direction, due to differences in timestamps, we introduce 2 new unknown variables into the set of navigational equations. Unless we have 2 or more satellites, adding that direction into consideration will increase the total number of unknowns and thus make the problem worse.

Finally, if the total number of acquired satellites (allowing repetition) in the combined acquisition is at least $2M+3$, we proceed to the location estimation phase. In Section 6, we describe how we obtain the $2M + 3$ formula.

4.3 Multi-Directional Location Estimation

The location estimation module takes the combined acquisition result as an input and computes the 3D coordinates of the indoor location. Recall that, to estimate the location, we need a precise timestamp and the ephemeris at that instant. We estimate the ms part of the timestamp from a nearby landmark, which is either generated (as done in CO-GPS) or previously known (e.g. a location outside of the building). The sub-ms part of the timestamp is obtained from the code phase, which comes as a byproduct of the acquisition process. The ephemeris is obtained directly from the web. Once we have all this information, we formulate a set of linear equations with $2M + 3$ unknowns and solve them using a least squares solver. The details of how we formulate the set of linear equations is described in Section 6.

5. ACQUISITION FROM WEAK SIGNALS

In this section, we, first, discuss the standard satellite acquisition process and, then, describe how to make it robust.

5.1 Standard Acquisition

After receiving GPS packets, a receiver first demodulates the signals and then passes the signals to the acquisition process. Figure 3 shows a simplified diagram of the satellite acquisition process of an Instant GPS. In order to identify the presence of a satellite, the receiver takes any 1 ms chunk of signals and computes the correlation between the signals and the universally known satellite-specific C/A code to find a match. Since the code phase is unknown, the receiver repeatedly shifts the C/A code circularly, and computes the correlation as in Equation 1:

$$\mathcal{R}[m] = \sum_{n=0}^{L-1} x[n].CA[(n+m)_L], 0 \leq m \leq L-1 \qquad (1)$$

where, $x[n]$, $CA[(n+m)_L]$, and $\mathcal{R}[m]$ denote the L-length signals, the C/A code which is shifted m places modulo L, and the m^{th} correlation, respectively. A correlation plot (code phase vs. correlation) is obtained by computing all $\mathcal{R}[m]$s. The unique highest peak in the plot signifies the presence of the satellite, whereas a flat line means the satellite is not acquired. The displacement of the peak in the plot is the code phase which gives us the sub-ms part of the propagation delay.

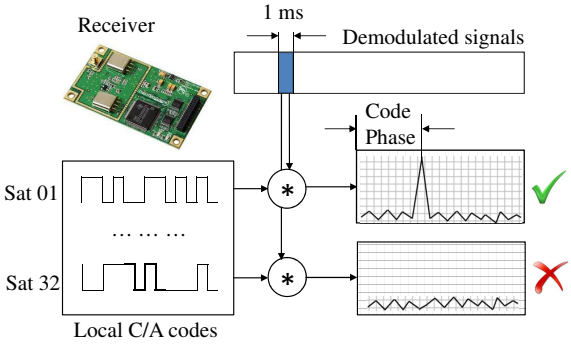

Figure 3: Simplified standard satellite acquisition.

One caveat is that the above algorithm does not deal with Doppler shifts which must be taken into account during acquisition. Taking Doppler effect into account is done simply by replicating the entire process, each time using a different frequency within the range of ±4.2 kHz of the carrier frequency. With this modification, the search space becomes a 2D state space consisting of all possible code phases and Doppler shifts. In our implementation, we use 25 frequency bins and process them in parallel to speed up the search.

5.1.1 FFT Search

Most commercial receivers use the above linear search algorithm for its simplicity. However, with computing correlation repeatedly being slow, we use a faster method in COIN-GPS, in which, correlations are computed with the help of FFT as shown in Equation 2. This is possible since Equation 1 resembles a convolution operation which is multiplication in the frequency domain. [38] shows that the FFT search is 2000x faster than the linear search algorithm.

$$\mathcal{R}[m] = x[n] * CA[-n] = \mathcal{F}^{-1}(\mathcal{F}(x[n]) \cdot \mathcal{F}(CA[n])^*) \qquad (2)$$

In order to find the unique peak in $\mathcal{R}[m], 0 \leq m \leq L-1$, the ratio of the maximum and the average (or, the second highest peak) of $\mathcal{R}[m]$ is taken, and if it is above a threshold ρ, the satellite is considered acquired. Because of the properties of the C/A codes (which are 1023-length Gold codes), ideally, only a non-delayed exact replica of a C/A code will produce a normalized correlation value of 1 (after dividing by the length 1023). For any other delays or any other satel-

lite's C/A code, the autocorrelation is close to zero, or more precisely one of these three values: $-1/1023$, $63/1023$, or $-65/1023$. Hence, a $\mathcal{R}[m]$ close to 1 and a $\rho > 2$ indicate that we have acquired the satellite.

5.2 Robust Acquisition

5.2.1 *Integrating Correlations*

In the presence of noise, the idealistic nature of $\mathcal{R}[m]$ does not hold, and detecting the right peak becomes non-trivial. In order to understand the effect of noise on peak $R[m]$, we perform an experiment, where we distort a GPS packet, obtained from a commercial GPS receiver, by artificially adding Gaussian noise (AWGN) and correlate it with a noise free C/A code. Figure 4 shows that as we vary the SNR from +15 dB to −60 dB, $\mathcal{R}[m]$ deviates from its ideal value of 1, and the peak ratio gets close to 1, which means that the highest peak becomes comparable to noise. Therefore, in indoor environments where SNR is below −30 dB, we won't be able to acquire any satellite with a regular GPS.

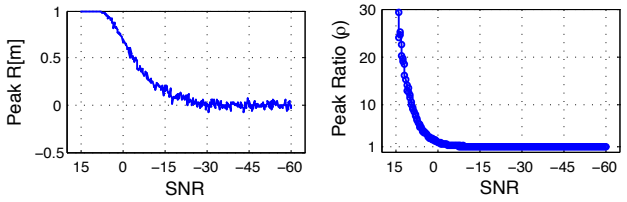

Figure 4: Effect of SNR on correlation peak.

With ≈ 10 dBi directional gain, a directional antenna helps reduce a great deal of noise. However, to complement its capability, we perform additional signal processing during acquisition. To further reduce noise, we use a non-coherent integrator to element-wise add correlations from consecutive 1 ms signal chunks. Assuming $\mathcal{R}^{(i)}[m]$ to be the correlation from the i^{th} chunk of 1 ms signals, the integrated correlations are obtained from Equation 3:

$$\mathcal{R}^2[m] = \sum_{i=1}^{K} |\mathcal{R}^{(i)}[m]|^2 \tag{3}$$

The effect of this integration is illustrated with an example in Figure 5. The first plot having $K = 1$ uses only 1 ms of signals to produce the correlation plot. The seemingly highest peak in this plot is labeled as the wrong peak, which becomes evident when we integrate correlations obtained from 2, 4, and 8 ms of signals in the next three plots. The reason the peak is clearer in the later plots is that, the highest peak remains at the same position while the noise varies. The more we integrate, the closer we get to the expected values and the more the variance is reduced.

Analysis: Assuming $E[\mathcal{R}]$ and $E[\mathcal{N}]$ to be the expected values of correlation power and squared noise, respectively, the expected value of peak ratio ρ is:

$$E[\rho] \approx \frac{K.E[\mathcal{N}] + K.E[\mathcal{R}]}{K.E[\mathcal{N}]} = 1 + \frac{E[\mathcal{R}]}{E[\mathcal{N}]} \tag{4}$$

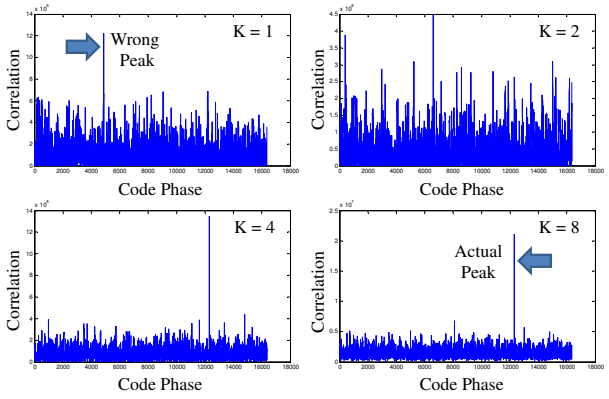

Figure 5: Longer integration produces a better peak.

This is consistent with the plot of ρ in Figure 4. For example, when a satellite is not present, $E[\mathcal{R}] = 0$ leads to an $E[\rho]$ of 1; otherwise, the ratio is dictated by the SNR.

5.2.2 *Data Bit Flip*

The duration of a data bit in a GPS packet is 20 ms. Hence, it is possible that a correlation peak will be lost during a data bit flip. This problem was solved in CO-GPS [22] by taking the maximum of two consecutive correlations. In COIN-GPS, however, due to non-coherent integration of correlator outputs, even if a peak is missed, it is compensated by other $K - 1$ values. Furthermore, as we add absolute values, there is no chance that a positive and a negative correlation will cancel each other in the event of a data bit transition.

6. INDOOR LOCATION ESTIMATION

Even after using a high-gain directional antenna and a robust acquisition algorithm, it is possible that the number of acquired satellites inside a building is inadequate. This section describes how we exploit the stationarity of an indoor receiver and handle the inadequate satellite problem by combining directional acquisitions.

6.1 Required Number of Satellites

The required number of satellites for location estimation equals the number of unknown variables. Theoretically, distances from three satellites should be enough to compute the receiver's (X, Y, Z) coordinates. Practically, however, in an instant GPS, two more satellites are required due to two more unknowns: the *common bias* and the *coarse time error*. Therefore, we need at least 5 acquired satellites to estimate the receiver's position.

6.1.1 *Common Bias Error*

The pseudo-range error due to the difference between a satellite's clock and a receiver's clock is the common bias. GPS satellites carry high-precision atomic clocks which are always in sync, and even the smallest drift in a satellite clock is included in the message, and hence, it is correctible. Receivers, on the other hand, use cheap, low-power, and small form-factored quartz crystal oscillators which have less pre-

cision and larger drifts. A 1 μs offset between the receiver and the satellite clock produces a pseudo-range error of 300 m. This bias term is estimated as an unknown parameter along with the receiver's position in the navigation solution. Figure 6 explains the common bias b for three satellites at a particular instant.

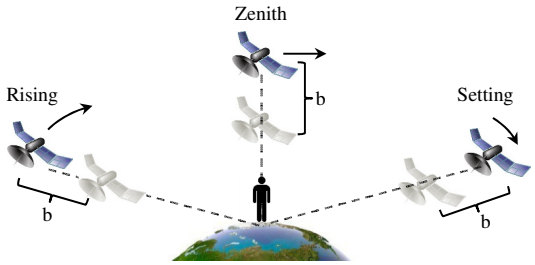

Figure 6: Common clock bias.

6.1.2 *Coarse Time Error*

In CTN, a coarse time reference from a nearby landmark is used, which results in another form of pseudo-range error called the coarse time error. Unlike the common bias which affects the measurements all by the same amount, coarse time error affects the pseudo-ranges, each by a different amount. Figure 7 illustrates this for a rising, a setting, and a satellite at the zenith. Due to coarse time offset, a rising satellite appears to be closer than its actual position, which results in a negative pseudo-range error. For a setting satellite, the error is positive, and a satellite at the zenith is free from this error. Although the coarse time error in terms of pseudo-range is different for each satellite, we know the velocity (pseudo-range rate) of each satellite from the ephemeris, so the error can be expressed as a product of the velocity and the unknown coarse time offset. Like common bias, the coarse time offset is also estimated as an unknown parameter in the navigation solution.

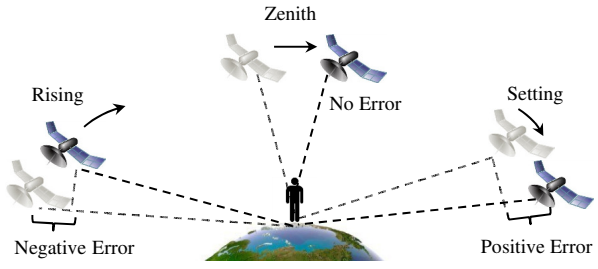

Figure 7: Coarse time error.

6.2 Handling Inadequate Satellites Indoors

A key assumption in COIN-GPS is that: the receiver's motion within a short period is so negligible that if we capture multiple time-delayed chunks of GPS signals within that interval, all chunks will result in the same (x, y, z) coordinates. With this assumption of a fixed (or, slow-moving) receiver, we can reuse the physical satellites that are acquired in more than one chunk. For example, if only the same 3 satellites are acquired in 3 chunks obtained in an indoor environment, no existing GPS receiver is able to estimate its position. However, COIN-GPS in such a case would acquire those 3 satellites 3 times each for a total of 9 satellite references, and can estimate the location.

Figure 8: Satellites move fast, the shopper barely moves.

Figure 8 depicts a scenario where a shopper is shopping at a convenience store. At 10:30 AM, when he is browsing a shelf, there happens to be 3 satellites that COIN-GPS acquires. After about half a second, the user's location is practically unchanged, but there are now 4 acquired satellites by COIN-GPS. From these two sets of satellites, which may or may not have any overlap, we formulate two sets of equations, S_1 and S_2 as shown in Equation 5 and Equation 6. Each element $E^{(k)}_{x_i y_i z_i b_i c_i}$ in S_i is an equation having 5 unknowns: the location coordinates (x_i, y_i, z_i), bias b_i, and the coarse time offset c_i. Since we must have at least 5 equations to solve for these 5 unknowns, none of the two sets individually can be used to estimate the variables. We have placed a question mark '?' explicitly to specify the absence of an equation.

$$S_1 = \left\{E^{(1)}_{x_1y_1z_1b_1c_1}, E^{(2)}_{x_1y_1z_1b_1c_1}, E^{(3)}_{x_1y_1z_1b_1c_1}, ?\,, ?\right\} \quad (5)$$

$$S_2 = \left\{E^{(4)}_{x_2y_2z_2b_2c_2}, E^{(5)}_{x_2y_2z_2b_2c_2}, E^{(6)}_{x_2y_2z_2b_2c_2}, E^{(7)}_{x_2y_2z_2b_2c_2}, ?\right\} \quad (6)$$

Under the stationary assumption, we set (x_1, y_1, z_1) and (x_2, y_2, z_3) equal, and thus reduce the total number of unknowns from 10 to 7. We now have 7 equations with 7 unknowns, and hence the combined set of equations in Eq. 7 is readily solvable with a least squares solver.

$$S_{12} = \left\{E^{(1)}_{xyzb_1c_1}, E^{(2)}_{xyzb_1c_1}, E^{(3)}_{xyzb_1c_1}, E^{(4)}_{xyzb_2c_2}, E^{(5)}_{xyzb_2c_2}, E^{(6)}_{xyzb_2c_2}, E^{(7)}_{xyzb_2c_2}\right\} \quad (7)$$

Note that a further reduction in the number of unknowns is possible if we could relate the bias and coarse time offset terms across S_1 and S_2. However, considering unpredictable delays between the start of capturing the signals and logging of timestamps inside the receiver, we decide to keep b_i's and c_i's as independent unknown variables. Generalizing this for M independent acquisitions, we are now ready to state our formula for a stationary receiver:

Stationary Instant GPS Formula 1. *For a stationary receiver, the required total number of visible GPS satellites for an instant GPS is $2M+3$, where M is the number of independent acquisitions and the same satellite acquired in different readings is considered different.*

Proof. Each time we consider a new set of acquired satellites, we add two unknowns: the bias and the coarse time offset for that instant. Thus, for M independent acquisitions, we have M bias terms, and M coarse time error terms. Including x, y, and z, which are common, we have a total of $2M + 3$ unknowns. Each acquired satellite contributes one equation involving $2M + 3$ unknowns. Hence, the required number of satellites is $2M + 3$. □

6.3 Navigation Equations

6.3.1 Standard Coarse Time Navigation

Like most navigation problems, CTN [37] uses an iterative approach to estimate the location (x, y, z) and the error terms: bias (b), and coarse time offset (tc). Let us define the state variable $\mathbf{p}$ having these 5 unknowns as: $\mathbf{p} = [x, y, z, b, tc]^T$. At each iteration, $\mathbf{p}$ is updated by the amount $\delta\mathbf{p} = [\delta_x, \delta_y, \delta_z, \delta_b, \delta_{tc}]$. The following 4 steps are iterated until $|\delta\mathbf{p}| \leq \epsilon$.

Step 1: Start with a priori estimate of $\mathbf{p}$. Initially, $\mathbf{p}_{xyz}$ is the reference location, and $\mathbf{p}_b$ and $\mathbf{p}_{tc}$ are zero.

Step 2: Predict the pseudo-range vector $\hat{\mathbf{z}}$ based on $\mathbf{p}$. The element $\hat{z}^{(k)}$ corresponds to the k^{th} acquired satellite.

Step 3: Measure the pseudo-range vector $\mathbf{z}$. The element $z^{(k)}$ corresponds to the k^{th} acquired satellite.

Step 4: Compute $\delta\mathbf{p}$ as a function of $\delta\mathbf{z} = \mathbf{z} - \hat{\mathbf{z}}$, and update the state variable $\mathbf{p}$.

The fourth step is where we relate the pseudo-range residuals $\delta z^{(k)}$ in terms of the spatial elements of $\delta\mathbf{p}$, i.e. $\delta\mathbf{p}_{xyz}$, the bias δ_b, and the coarse time offset δ_{tc}, all having the units of distance.

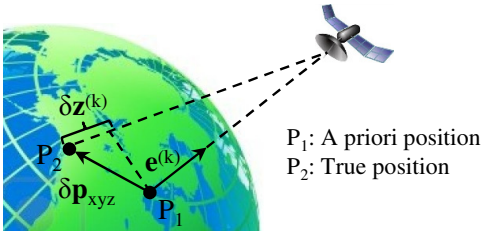

Figure 9: A priori and true location.

The pseudo-range error due to the spatial elements of $\delta\mathbf{p}$ is illustrated in Figure 9. For each satellite, the error $\delta z^{(k)}$ is expressed by $-\mathbf{e}^{(k)} \cdot \delta\mathbf{p}_{xyz}$, where $\mathbf{e}^{(k)}$ is the unit vector from the priori location estimate P_1 to the k^{th} satellite's position. The bias term δ_b, which is a distance term and is the same for all satellites, is simply added to the error. The coarse time error is expressed by, $-\nu^{(k)} \cdot \delta_{tc}$, where $\nu^{(k)}$ is the pseudo-range rate which is obtained from the velocity information of each satellite found in the Ephemeris data. Thus, for each satellite, the relationship between $\delta z^{(k)}$ and $\mathbf{p}$ is:

$$\delta z^{(k)} = -\mathbf{e}^{(k)} \cdot \delta\mathbf{p}_{xyz} + \delta_b + \nu^{(k)} \cdot \delta_{tc} \tag{8}$$

Using matrix notations, the above equation, considering M visible satellites is expressed by,

$$\delta\mathbf{z} = \mathbf{H} \cdot \delta\mathbf{p} \tag{9}$$

where

$$\mathbf{H} = \begin{bmatrix} -e^{(1)} & 1 & \nu^{(1)} \\ \vdots & \vdots & \vdots \\ -e^{(M)} & 1 & \nu^{(M)} \end{bmatrix} \tag{10}$$

Finally, we get $\delta\mathbf{p}$ using the standard least squares solution:

$$\delta\mathbf{p} = (\mathbf{H}^T\mathbf{H})^{-1}\mathbf{H}^T \cdot \delta\mathbf{z} \tag{11}$$

6.3.2 Indoor Navigation Equations

Let us assume that, there are M directional acquisitions having $K_1, K_2, \ldots K_M$ acquired satellites, respectively. Throughout this section, we use the superscript (i, k) to denote the k^{th} satellite in i^{th} chunk, where $1 \leq i \leq M$ and $1 \leq k \leq K_i$. Before we derive an expression for the pseudo-range error $\delta z^{(i,k)}$, we make the following assumptions:

- The (x, y, z) coordinates are the same in all chunks.
- Each chunk has a bias b_i and a coarse time error tc_i.
- Total number of satellites $\sum_{j=1}^{M} K_j \geq 2M + 3$.

Generalizing Equation 8 we obtain:

$$\delta z^{(i,k)} = -\mathbf{e}^{(i,k)} \cdot \delta\mathbf{p}_{xyz} + \delta_{b_i} + \nu^{(i,k)} \cdot \delta_{tc_i} \tag{12}$$

Considering all K_i satellites in i^{th} chunk:

$$\delta\mathbf{z}^{(\mathbf{i})} = \mathbf{H}^{(\mathbf{i})} \cdot \delta\mathbf{p}^{(\mathbf{i})} \tag{13}$$

where

$$\mathbf{H}^{(\mathbf{i})} = \begin{bmatrix} -e^{(i,1)} & 1 & \nu^{(i,1)} \\ \vdots & \vdots & \vdots \\ -e^{(i,K_i)} & 1 & \nu^{(i,K_i)} \end{bmatrix} \tag{14}$$

Extending the state variable $\mathbf{p}$ by including all $(2M + 3)$ variables, for $\mathbf{p} = [x, y, z, b_1, tc_1, \ldots b_M, tc_M]^T$, we rewrite the above equation as:

$$\mathbf{H}^{(\mathbf{i})} = \begin{bmatrix} -e^{(i,1)} & 0 & 0 & \ldots & 1 & \nu^{(i,1)} & \ldots & 0 & 0 \\ \vdots & \vdots & \vdots & & \vdots & \vdots & & \vdots & \vdots \\ -e^{(i,K_i)} & 0 & 0 & \ldots & 1 & \nu^{(i,K_i)} & \ldots & 0 & 0 \end{bmatrix} \tag{15}$$

Stacking up all $\mathbf{H}^{(\mathbf{i})}$, $1 \leq i \leq M$, we get the observation matrix $\mathbf{H}$ for indoor navigation:

$$\mathbf{H} = \begin{bmatrix} -e^{(1,1)} & 1 & \nu^{(1,1)} & \ldots & 0 & 0 \\ \vdots & \vdots & \vdots & & \vdots & \vdots \\ -e^{(1,K_1)} & 1 & \nu^{(1,K_1)} & \ldots & 0 & 0 \\ \vdots & \vdots & \vdots & & \vdots & \vdots \\ -e^{(M,1)} & 0 & 0 & \ldots & 1 & \nu^{(M,1)} \\ \vdots & \vdots & \vdots & & \vdots & \vdots \\ -e^{(M,K_M)} & 0 & 0 & \ldots & 1 & \nu^{(M,K_M)} \end{bmatrix} \tag{16}$$

Finally, we obtain $\delta\mathbf{p}$ by using the standard least squares solution as done in Equation 11.

7. SYSTEM IMPLEMENTATION

So far we have provided a generic description of how an indoor GPS could be built. This section describes the specific implementation of COIN-GPS.

7.1 Front End Hardware

The front-end of COIN-GPS consists primarily of three components: a high-gain directional antenna, the direction controller, and a GPS signal logger, which are connected to a PC as shown in Figure 10.

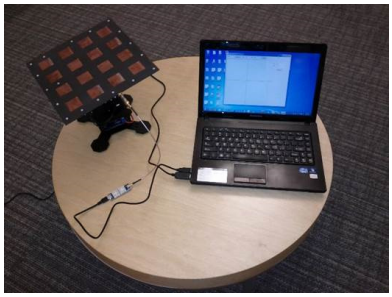

Figure 10: The antenna and the signal logger are connected to a PC.

7.1.1 *Antenna Design*

In order to have a reasonable gain and also a reasonable size of the antenna, we build an antenna with a 4×4 array of patches that has the dimensions of 10×10 inch^2 and a thickness of < 0.5 inch. The antenna has a directional gain of 12.3 dBi, a half-power beam width of 35°, and a broadside angle of 0.5°. Figure 11(a) shows the simulated gain of the antenna in 3D. The antenna is directional, which means it receives signals along it's Z-axis, and the receiving direction is controllable. Figure 11(b) shows that it's receiving frequency is 1.575 GHz corresponding to the GPS.

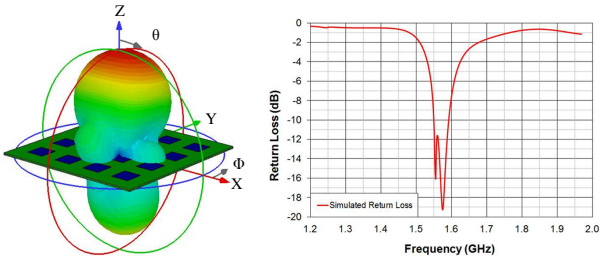

(a) Antenna Beam (b) Return Loss

Figure 11: Antenna Beam and Return Loss.

The antenna is composed of a couple of two-layer boards (boards with two copper layers and one substrate layer) that are physically connected to each other by plastic screws. The substrate used for each two-layer board is RT/Duroid 5880. Its low dielectric constant ($\epsilon_r = 2.2$) and low loss tangent ($\tan\delta = 0.0009$) is the most suitable substrate for producing maximal gain for a given patch antenna topology. One of the boards (Board A) consists of a ground layer that is filled with 16 coupling slots (one for each patch antenna) and a corporate feeding network. The other board (Board B) has an analogous ground layer, filled with 16 coupling slots, and a layer with 16 patches. The size of each patch is 1.25×1.25 inch^2. The antenna operates by, first, exciting a current on the feeding network of Board A. When that current reaches the feed-line directly below the coupling slot, energy is electromagnetically coupled through this aperture on the ground plane of both boards to the patch of Board B and radiated into free space.

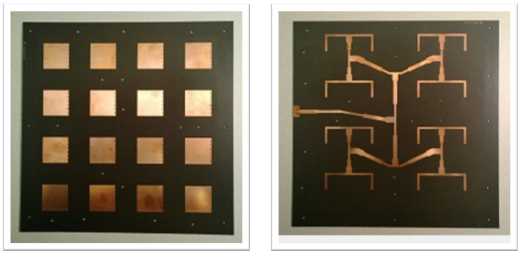

(a) Antenna Front (b) Antenna Back

Figure 12: Front and Back of the Antenna

7.1.2 *Steering the Antenna*

In COIN-GPS, we attempt to receive GPS signals from a total of nine main beam directions with respect to the X-Z and Y-Z elevation planes. These directions are denoted by coordinates (R, S) where R is the main beam tilt angle along the X-axis, and S is the tilt angle along the Y-axis. The directions are $(0, 0)$, $(\pm 15, 0)$, $(\pm 30, 0)$, $(0, \pm 15)$, and $(0, \pm 30)$.

We use a programmable mechanical robot to control the antenna's direction by rotating it physically. The antenna is mounted on top of a mechanical pan-tilt platform, WidowX Robot Turret [3], which provides 360° rotation to steer the antenna at any direction. During operation, the antenna is pointed towards different directions, and from each direction, we collect raw GPS signals using a GPS signal sampler.

7.1.3 *GPS Signal Sampler*

We use an off-the-shelf GPS signal sampler, SiGe GN3S Sampler v3 [2]), that connects to the USB port of a laptop. The sampler has an MCX antenna connector port where we connect our high-gain antenna. The sampler directly captures low-level GPS signals at 16368 samples/ms at the intermediate frequency of 4.092 MHz, and sends the samples directly to the laptop. The laptop simultaneously controls the robot, and the GPS signal sampler collects 100 ms of GPS samples from each of the nine directions and stores them into the disk for processing.

7.2 Back End Software

Due to space limitations, we discuss the back-end processing of COIN-GPS in brief. The two main tasks of the back-end are to maintain an up-to-date ephemeris database and to run the algorithms that are described in Section 5 and Section 6. We use the precise ephemeris from the National Geospatial-Intelligence Agency (NGA). All of our web services corresponding to the ephemeris, acquisition, and loca-

tion estimation are written in C#, and are deployed in the Windows Azure cloud.

We choose to run our algorithms in the cloud because, first, signal processing is costly and especially our proposed robust acquisition algorithm has 10 – 100 times more processing overhead (for its best result) which is not suitable for an embedded platform due to timing and energy constraints. Instead, it is done in the cloud to take advantage of its parallel processing capability which makes COIN-GPS both fast and energy efficient. Second, in an instant GPS technique we must use a web service to get ephemeris data anyway, so we believe having the signal processing tasks as part of a cloud-service is the right design choice.

8. EVALUATION

We describe a series of experiments which are categorized into four types: execution time, robustness of acquisition, location estimation, and five case studies.

8.1 Experimental Setup

We perform an in-depth evaluation of COIN-GPS by deploying the system in four single-storied stores (Starbucks, Home Depot, Fred Meyer, and Costco) and one multi-storied shopping mall (Bellevue Square Mall) which are located in the Bellevue, WA. Inside each building, we capture and log GPS signals from 2 – 16 locations, using COIN-GPS, and a baseline Garmin GPS logger. At each location, COIN-GPS steers its antenna towards nine different directions, and logs 100 ms of GPS signals from each direction. The baseline Garmin device also logs 100 ms signals at each location.

To obtain the ground truth, we use a laser-based distance measurement device that has a range of 100 feet with 1/8 inch accuracy. At each location inside a building, we shoot the laser pointer to at least two nearby walls, so that we can identify the location later on Bing maps, and thus obtain the true latitude and longitude of the location. To be able to exactly pin-point the location on the map, we often have chosen locations that are near a corner, or a junction, or in the middle of a section of the store that is identifiable on a map (e.g. frozen foods in Costco). Some of the stores (e.g. Home Depot and Bellevue Square Mall) provided us with their floor-plans which also helped us identify the spots.

8.2 Execution Time

We measure the execution times of different components in COIN-GPS and summarize them in Table 1. Each time the front-end antenna is steered to a particular direction, it takes about 100 ms to settle down. Collecting 100 ms signals and storing them takes an additional 200 ms. Considering nine directions, it takes about 3 seconds to complete one cycle of data logging. The back-end server that we have used is a Windows Server 2008 R2 PC having a Quad Core CPU @ 3.3 GHz and 16 GB RAM. The acquisition module takes 1.8 s per ms signals, i.e. for the maximum 100 ms signals and assuming no parallel processing, the worst case acquisition time is as high as 3 mins. The overhead is a one-time cost consisting of loading the C/A code tables, preparing caches, and ephemeris data, which require an update once a day. Compared to acquisition, location estimation is faster and takes 1.33 s on average. Overall, with parallelism, the end-to-end time is about 3.13 s. Without parallelism and a moderate 20 – 50 ms signals, the time it about 40 – 90 s, which is in the same order of magnitude of GPS receivers in outdoor environments - 30 to 60 s for standalone GPS and 6+ s for AGPS.

Task	Module	Time (sec)
Front-End	Settling Time (per direction)	0.10
	Data Logger (per direction)	0.20
Acquisition	Acquire (per ms signal)	1.80
	Other Overhead (one time)	3.50
Localization	Estimate Location (per fix)	1.33

Table 1: Modules and Execution Times.

8.3 Robustness of Acquisition

8.3.1 Longer Signals and Acquired Satellites

In Section 5.2.1, we have described the benefit of integrating correlations from more than 1 ms of signals. In this experiment, we quantify this using our empirical data. Figure 13 shows the number of satellites acquired by both COIN-GPS and the Garmin device, as we vary the amount of signals over which we integrate the correlation. We observe that the number of acquired satellites increases in both cases, however, COIN-GPS acquires 3 satellites (on average) when we integrate 50 or more correlation terms (shaded region in the figure). For the Garmin device, the average number hardly ever reaches 2, even when we integrate over 100 ms. The state-of-the-art CO-GPS (or any instant GPS), which uses 1 – 2 ms signals, does not acquire even a single satellite. Thus, this result justifies the use of our high-gain directional antenna as well as our robust acquisition technique, which lets COIN-GPS acquire enough satellites to obtain a location fix in an indoor environment.

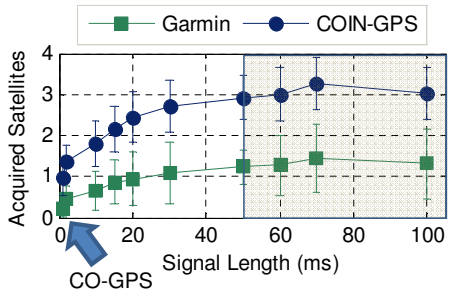

Figure 13: Signal length and acquired satellites.

The underlying reason that using a longer signal length helps is understood when we plot the peak ratios of a correlation plot for different amount of signals. Figure 14(a) shows that as we increase the amount of signals over which

we integrate the correlation, the ratio between the highest two peaks (peak ratio) increases. However, after 50 ms, the increase is not significant and settles at around 7. Therefore, this number is used as a threshold in determining whether or not a satellite is acquired.

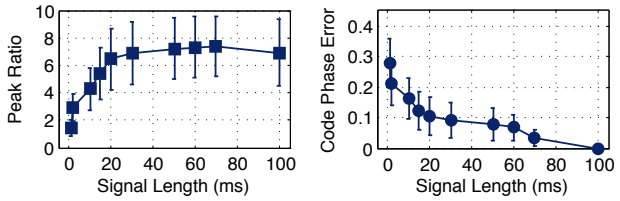

(a) Peak ratio. (b) Code phase error.

Figure 14: Peak ratio and code phase error.

Another important thing to notice is the errors in estimated code phases as we consider longer signals. This is because, ultimately, it is the code phase estimation error that determines the location estimation error in an instant GPS receiver by and large. Figure 14(b) shows that the relative code phase error diminishes as more and more correlation terms are integrated and becomes less than 5% when 70 or more correlation terms are integrated. Hence, this plot provides a guide in selecting a value of signal length to minimize the expected location estimation error. In COIN-GPS, we use 50 ms as our default integration length.

8.3.2 Indoor Satellite Distribution

COIN-GPS requires acquisition of at least 3 satellites to obtain a location fix. In this experiment, we empirically determine the distribution of the number of acquired satellites (from a single direction in COIN-GPS) for both COIN-GPS and a CO-GPS (having a Garmin device as a front-end). Figure 15 shows that, although CO-GPS acquires 2 or more satellites with only 10% probability, it never acquires 3 satellites and never obtains a location fix. On the other hand, COIN-GPS acquires at least 3 satellites 60% of the time which means, COIN-GPS is capable of obtaining a location fix in these cases. Compared to the state-of-the-art CO-GPS's 0% success rate, this is a significant improvement.

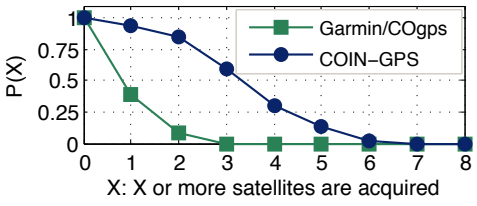

Figure 15: Distribution of acquired satellites.

8.4 Location Estimation Algorithm Evaluation

8.4.1 Combining Directional Acquisitions

COIN-GPS combines acquired satellites from up to nine directions to address the inadequate satellite problem. We empirically determine the number of directional acquisitions that are combined in COIN-GPS whenever there has been a successful location fix. Figure 16 shows the CDF of the number of directions combined. We see that, amongst all successful fixes, 63% use only one direction, 28% use 2, and 3 directions are required for the rest.

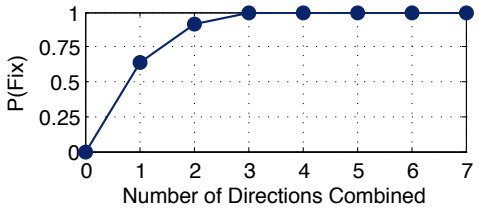

Figure 16: Distribution of location fixes.

8.4.2 Bias and Coarse Time Error Terms

In COIN-GPS, for M independent directional acquisitions, we assume there are M unknown bias terms and M unknown coarse time error terms. In this experiment, our goal is to see how different the biases and the coarse time offsets are and thus justify the assumption.

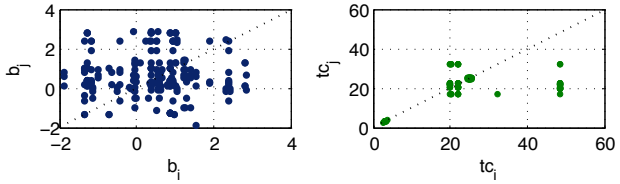

(a) bias ($\times 10^5$ m) (b) coarse time (ms)

Figure 17: Bias and Coarse Time.

Figure 17 shows all-pair biases and coarse time offsets obtained after solving the navigational equations. Each point (b_i, b_i) in Figure 17(a) represents two bias terms b_i and b_j from the same set of equations. Similarly, Figure 17(b) shows the coarse time offsets in pairs. If all M biases (or all M coarse time errors) were the same, the plot would be a straight line with a slope of 1. However, we see that the biases are highly scattered and most of the coarse time offsets are off the diagonal line. Making all M biases and all M coarse term offsets the same would result in estimated pseudo-range errors of 410 m and 25 m, respectively. Hence, by considering them as $2M$ independent unknown variables, COIN-GPS has eliminated such large errors.

8.5 Location Estimation Case Studies

We deploy COIN-GPS in five real-world indoor environments and summarize the results in Figures 18−21. In each figure, a pair of downward arrows on the map show the true and estimated locations, and the dotted line shows the displacement. The table on the right compares COIN-GPS with the baseline, and the plot shows the localization errors.

COIN-GPS performs its best at Starbucks (Figure 18) and Home Depot (Figure 19), showing a 100% success rate in obtaining a location fix. These places are suitable for COIN-GPS as in Starbucks, there is a large window at the front, and there are several skylights in Home Depot which

System	Locations	Fixes
Garmin	2	None
COIN-GPS	2	2

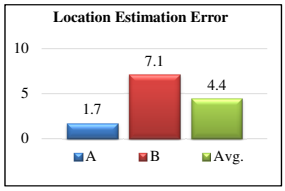

Figure 18: Starbucks.

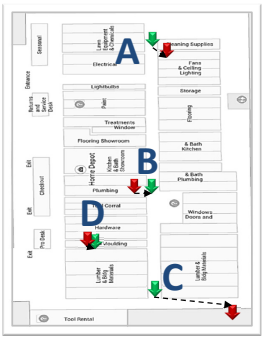

System	Locations	Fixes
Garmin	4	None
COIN-GPS	4	4

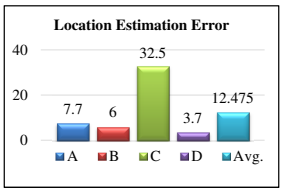

Figure 19: Home Depot.

are made of glass and framed with steel. On average, COIN-GPS acquires 3.5 satellites per direction in both locations, and obtains location fixes with 4.4−12.5 m errors. With such errors, we can distinguish between a customer at Starbucks waiting in the line versus a customer sitting in the deep back of the store. We can also identify the section a customer is in Home Depot (e.g. cleaning, plumbing, moulding, or lumber). The baseline Garmin device, on the other hand, sees < 1 satellite on average, and never gets a location fix.

System	Locations	Fixes
Garmin	16	None
COIN-GPS	16	9

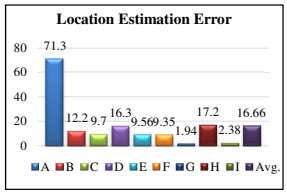

Figure 20: Bellevue Square Mall (two storied).

The Bellevue Square Mall (Figure 20) is a large, multi-storied shopping mall. We conduct our experiment on its first and the second floors where a large walking area on the first floor shares the same roof with the top floor. Starting from A on the second floor, we take measurements from 8 spots on the second floor, 8 on the first floor, and stop at I. We get 6 successful fixes ($A - F$) on the second floor, and 3 on the first ($G - I$) with average errors of 21 m and 7.17 m, respectively. We get higher errors on the second floor (e.g. A) than the first (e.g. I) as sometimes the signals are reflected by the lower floor before they reach the top floor. Garmin receiver, on the other hand, hardly acquires a satellite at any spot and hence does not get any location fix.

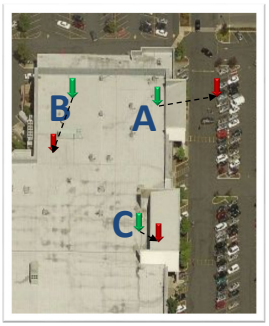

System	Locations	Fixes
Garmin	5	None
COIN-GPS	5	3

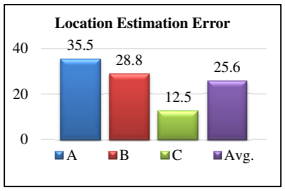

Figure 21: Fred Meyer.

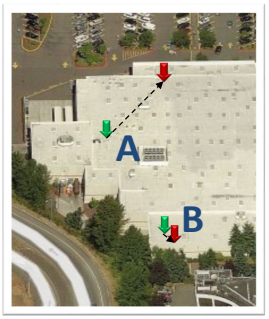

System	Locations	Fixes
Garmin	4	None
COIN-GPS	4	2

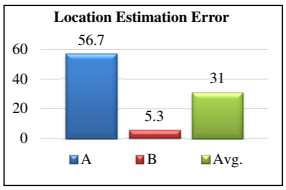

Figure 22: Costco.

The two most difficult cases for COIN-GPS have been the Fred Meyer (Figure 21) and the Costco (Figure 22). These buildings are somewhat sealed, having a ceiling made of concrete and a thick layer of steel framework, and they have no skylights. Out of a total of 9 spots inside these two buildings, COIN-GPS obtains 5 successful location fixes with an aggregate average error of 27.6 m. The received signals inside these buildings are so weak that COIN-GPS acquires 3 or more satellites in only about 30% of the directional acquisitions. The Garmin device acquires absolutely no satellite at all in these locations. Although COIN-GPS has its largest error in these scenarios, still the result is remarkable as it is capable of getting a location fix when the state-of-the-art does not even see a satellite.

Table 2 shows the overall min, median, mean, 90-th percentile, and max error in our study.

Min	Median	Mean	P90	Max
1.70	9.63	17.37	46.10	71.30

Table 2: Summary of Localization Errors.

9. DISCUSSION

Steering Antenna Electronically: Instead of using a programmable robot to steer the antenna physically, a more convenient alternative is to steer the beam electronically. We have implemented a prototype of such an electronically steerable antenna and tested its capability at a limited scale. As

it was not used in our deployment experiments, we do not include this design while describing our implementation. Instead, we discuss it here for the interested readers.

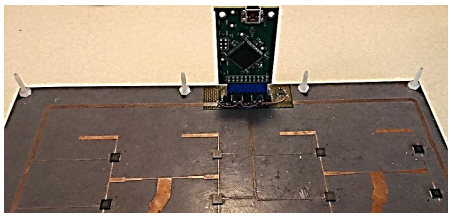

Figure 23: Electronically controllable antenna.

In Figure 23, the corporate feeding network is designed to provide excitation 'in-phase' to all 16 patches. When this 'in-phase' excitation occurs, the radiation pattern is broadside with maximal gain at around 0°. To enhance the reception of signals at different angles away from broadside without physically maneuvering the antenna, 16 voltage-controlled phase shifters (one for each antenna) are integrated to the network. The phase shifters offer 360° of phase delay controlled by a voltage that ranges from $0 - 13$ V. By changing these control voltages, the phases of the individual patches are shifted, and, in turn, the main beam of the radiation pattern is tilted. The voltage-controlled phase shifters are controlled by an externally-connected PCB that has a programmable SoC, and is powered through a USB cable connected to a laptop. By changing the duty cycle of a pulse-width modulated (PWM) voltage signal, different voltages between $0 - 13$ V are used to control the phase shifter. The PSoC allows 256-bit addressing; therefore, the control voltage increment for the phase shifter is ≈ 0.05 V.

Size of the Antenna: Compared to today's GPS receivers, which comfortably fit inside handheld devices, COIN-GPS along with its antenna are several orders of magnitude larger. This is a price that we are paying to compensate for the signal attenuation and multi-path effects that we incur indoors. However, since we have chosen a 10×10 inch^2 board having a thickness < 1 cm, the board with the electronically steerable antenna, at its current scale, can be fit nicely on the back-cover of a laptop.

Usage in Indoor Mapping: COIN-GPS, in its current form, is not really suitable to be commercialized and sold as a consumer product. However, the system has other applications, such as providing the ground-truth for other indoor profiling techniques, or mapping indoor environments similar to Google's street-view car or Bing's NAVTEQ system that are used outdoors. A limitation of COIN-GPS is that, in general, it does not work in multi-storied buildings. However, in a country like the USA, there are many single-storied buildings, such as stores, marts, warehouses, malls, schools, stations, and airports where COIN-GPS is usable.

Complementing COIN-GPS: COIN-GPS does not provide a guaranteed location fix at all times. Rather, it is highly likely that there will be several zones in a building where COIN-GPS may not acquire the required number of satellites. To handle such cases, relative location estimation techniques such as dead-reckoning [8, 40, 41] can be used to estimate locations between two consecutive fixes.

10. RELATED WORK

The GPS has been an active area of research ever since it was invented during the Cold War era. Our work in this paper is based on a rich body of work in GPS [24], A-GPS [37], and CO-GPS [22]. In particular, we adopt the concept of cloud-offloading from CO-GPS to save energy, however, our proposed front-end hardware, robust acquisition, and location estimation techniques are completely new and tailored to indoor environments. While we are the first to demonstrate an indoor GPS receiver that works in practical situations, there are some works that discuss indoor GPS challenges and opportunities [36, 35, 13, 4], signal characteristics [19], and achieving high-sensitivity [5, 42].

Several indoor positioning systems have been proposed in the past. There are surveys [16, 21] that summarize, compare and contrast some early efforts on indoor localization. Techniques used in state-of-the-art indoor positioning systems include fingerprinting WiFi RSS (Radar [7], Horus [43], Large scale 802.11 [17], EZ [11], WiGEM [15], and ZEE [29]), ultrasonic beacons (Cricket [28]), acoustics and ambience fingerprinting (BatPhone [33] and SurroundSense [6]), RFID (LandMarc [26]), and computer vision (SLAM [25], depth camera [9, 32]). All these systems have limitations, such as requiring an infrastructure setup and/or a characterization phase, and none of them provide a direct mapping to the real-world coordinates.

COIN-GPS, compared to the techniques mentioned above, does not require any extra infrastructure other than the existing GPS satellites, does not require any learning or characterization phase, and provides globally recognized GPS coordinates. Some techniques are complementary to COIN-GPS. For example, pedestrian dead-reckoning techniques [8, 40, 41] or hybrid approaches like UnLoc [39] and GAC [44] can be used along with COIN-GPS to handle the corner cases where COIN-GPS does not get a location fix.

11. CONCLUSION

In this paper, we challenge the common belief that GPS receivers cannot work indoors due to weak signals and multipath effects. By incorporating a steerable directional antenna, leveraging the computing power of the cloud for robust acquisitions over long signals, and combining acquisition results from different directions over time, we devise a novel way of performing direct GPS-based localization in indoor environments. The COIN-GPS system has been shown to achieve acceptable location accuracy without any additional infrastructure in several real-world single-storied public spaces. While the current implementation is limited by its size and accuracy, the results are remarkable as there have been no other GPS receivers that have achieved this much success. We believe this work will be the basis for future portable, consumer grade indoor GPS receivers.

12. REFERENCES

[1] CST Microwave Studio. www.cts.com.

[2] SiGe GN3S Sampler. sparkfun.com/products/10981.

[3] WidowX Robot Turret. www.trossenrobotics.com.

[4] N. Agarwal, J. Basch, P. Beckmann, P. Bharti, S. Bloebaum, S. Casadei, A. Chou, P. Enge, W. Fong, N. Hathi, et al. Algorithms for gps operation indoors and downtown. *GPS solutions*, 6(3):149–160, 2002.

[5] D. Akopian. Fast fft based gps satellite acquisition methods. *IEE Proceedings-Radar, Sonar and Navigation*, 152(4):277–286, 2005.

[6] M. Azizyan, I. Constandache, and R. Roy Choudhury. SurroundSense: mobile phone localization via ambience fingerprinting. In *MobiCom '09*, Beijing, China.

[7] P. Bahl and V. N. Padmanabhan. Radar: An in-building rf-based user location and tracking system. In *INFOCOM 2000. Nineteenth Annual Joint Conference of the IEEE Computer and Communications Societies. Proceedings. IEEE*, volume 2, pages 775–784. Ieee, 2000.

[8] S. Beauregard and H. Haas. Pedestrian dead reckoning: A basis for personal positioning. In *Proceedings of the 3rd Workshop on Positioning, Navigation and Communication (WPNCŠ06)*, pages 27–35, 2006.

[9] J. Biswas and M. Veloso. Depth camera based indoor mobile robot localization and navigation. In *Robotics and Automation (ICRA), 2012 IEEE International Conference on*, pages 1697–1702. IEEE, 2012.

[10] Y. Chen, D. Lymberopoulos, J. Liu, and B. Priyantha. Fm-based indoor localization. In *Proceedings of the 10th International Conference on Mobile Systems, Applications, and Services*, MobiSys '12, pages 169–182, New York, NY, USA, 2012. ACM.

[11] K. Chintalapudi, A. Padmanabha Iyer, and V. N. Padmanabhan. Indoor localization without the pain. In *Proceedings of the sixteenth annual international conference on Mobile computing and networking*, pages 173–184. ACM, 2010.

[12] J. Chung, M. Donahoe, C. Schmandt, I.-J. Kim, P. Razavai, and M. Wiseman. Indoor location sensing using geo-magnetism. In *Proceedings of the 9th International Conference on Mobile Systems, Applications, and Services*, MobiSys '11, pages 141–154, New York, NY, USA, 2011. ACM.

[13] G. Dedes and A. G. Dempster. Indoor gps positioning. In *Proceedings of the IEEE Semiannual Vehicular Technology Conference*, 2005.

[14] T. Denidni and Q. Rao. Design of single layer broadband slot antennas. *Electronics Letters*, 40(8):461–463, 2004.

[15] A. Goswami, L. E. Ortiz, and S. R. Das. Wigem: a learning-based approach for indoor localization. In *Proceedings of the Seventh COnference on emerging Networking EXperiments and Technologies*, page 3. ACM, 2011.

[16] Y. Gu, A. Lo, and I. Niemegeers. A survey of indoor positioning systems for wireless personal networks. *Communications Surveys & Tutorials, IEEE*, 11(1):13–32, 2009.

[17] A. Haeberlen, E. Flannery, A. M. Ladd, A. Rudys, D. S. Wallach, and L. E. Kavraki. Practical robust localization over large-scale 802.11 wireless networks. In *Proceedings of the 10th annual international conference on Mobile computing and networking*, pages 70–84. ACM, 2004.

[18] X. Jiang, C.-J. M. Liang, K. Chen, B. Zhang, J. Hsu, J. Liu, B. Cao, and F. Zhao. Design and evaluation of a wireless magnetic-based proximity detection platform for indoor applications. In *Proceedings of the 11th International Conference on Information Processing in Sensor Networks*, IPSN '12, pages 221–232, New York, NY, USA, 2012. ACM.

[19] M. B. Kjærgaard, H. Blunck, T. Godsk, T. Toftkjær, D. L. Christensen, and K. Grønbæk. Indoor positioning using gps revisited. In *Pervasive Computing*, pages 38–56. Springer, 2010.

[20] R. Li, G. DeJean, M. M. Tentzeris, and J. Laskar. Development and analysis of a folded shorted-patch antenna with reduced size. *Antennas and Propagation, IEEE Transactions on*, 52(2):555–562, 2004.

[21] H. Liu, H. Darabi, P. Banerjee, and J. Liu. Survey of wireless indoor positioning techniques and systems. *Systems, Man, and Cybernetics, Part C: Applications and Reviews, IEEE Transactions on*, 37(6):1067–1080, 2007.

[22] J. Liu, B. Priyantha, T. Hart, H. S. Ramos, A. A. Loureiro, and Q. Wang. Energy efficient gps sensing with cloud offloading. In *SenSys*, pages 85–98, 2012.

[23] D. López de Ipiña, P. R. S. Mendonça, and A. Hopper. Trip: A low-cost vision-based location system for ubiquitous computing. *Personal Ubiquitous Comput.*, 6(3):206–219, Jan. 2002.

[24] P. Misra and P. Enge. Global positioning system: Signals, measurements and. 2011.

[25] M. Montemerlo, S. Thrun, D. Koller, and B. Wegbreit. FastSLAM: A factored solution to the simultaneous localization and mapping problem. In *AAAI/IAAI*, pages 593–598, 2002.

[26] L. M. Ni, Y. Liu, Y. C. Lau, and A. P. Patil. Landmarc: indoor location sensing using active rfid. *Wireless networks*, 10(6):701–710, 2004.

[27] D. M. Pozar. Microstrip antennas. *Proceedings of the IEEE*, 80(1):79–91, 1992.

[28] N. B. Priyantha, A. Chakraborty, and H. Balakrishnan. The cricket location-support system. In *Proceedings of the 6th annual international conference on Mobile computing and networking*, pages 32–43. ACM, 2000.

[29] A. Rai, K. K. Chintalapudi, V. N. Padmanabhan, and R. Sen. Zee: Zero-effort crowdsourcing for indoor localization. In *Proceedings of the 18th annual international conference on Mobile computing and networking*, pages 293–304. ACM, 2012.

[30] S. K. Rao. Parametric design and analysis of multiple-beam reflector antennas for satellite communications. *Antennas and Propagation Magazine, IEEE*, 45(4):26–34, 2003.

[31] M. Redzic, C. Brennan, and N. E. O'Connor. Dual-sensor fusion for indoor user localisation. In *Proceedings of the 19th ACM International Conference on Multimedia*, MM '11, pages 1101–1104, New York, NY, USA, 2011. ACM.

[32] J. Shotton, T. Sharp, A. Kipman, A. Fitzgibbon, M. Finocchio, A. Blake, M. Cook, and R. Moore. Real-time human pose recognition in parts from single depth images. *Communications of the ACM*, 56(1):116–124, 2013.

[33] S. P. Tarzia, P. A. Dinda, R. P. Dick, and G. Memik. Indoor localization without infrastructure using the acoustic background spectrum. In *Proceedings of the 9th international conference on Mobile systems, applications, and services*, pages 155–168. ACM, 2011.

[34] G. Thiele. Analysis of yagi-uda-type antennas. *Antennas and Propagation, IEEE Transactions on*, 17(1):24–31, 1969.

[35] F. van Diggelen. Indoor gps theory & implementation. In *Position Location and Navigation Symposium, 2002 IEEE*, pages 240–247. IEEE, 2002.

[36] F. van Diggelen and C. Abraham. Indoor gps technology. *CTIA Wireless-Agenda, Dallas*, 2001.

[37] F. S. T. Van Diggelen. *A-gps: Assisted GPS, GNSS, and SBAS*. Artech House, 2009.

[38] D. Van Nee and A. Coenen. New fast gps code-acquisition technique using fft. *Electronics Letters*, 27(2):158–160, 1991.

[39] H. Wang, S. Sen, A. Elgohary, M. Farid, M. Youssef, and R. R. Choudhury. No need to war-drive: Unsupervised indoor localization. In *Proceedings of the 10th international conference on Mobile systems, applications, and services*, pages 197–210. ACM, 2012.

[40] O. Woodman and R. Harle. Pedestrian localisation for indoor environments. In *Proceedings of the 10th international conference on Ubiquitous computing*, pages 114–123. ACM, 2008.

[41] O. Woodman and R. Harle. Rf-based initialisation for inertial pedestrian tracking. In *Pervasive Computing*, pages 238–255. Springer, 2009.

[42] C. Yang, T. Nguyen, E. Blasch, and M. Miller. Post-correlation semi-coherent integration for high-dynamic and weak gps signal acquisition. In *Position, Location and Navigation Symposium, 2008 IEEE/ION*, pages 1341–1349. IEEE, 2008.

[43] M. Youssef and A. Agrawala. The horus wlan location determination system. In *Proceedings of the 3rd international conference on Mobile systems, applications, and services*, pages 205–218. ACM, 2005.

[44] M. Youssef, M. A. Yosef, and M. El-Derini. Gac: Energy-efficient hybrid gps-accelerometer-compass gsm localization. In *Global Telecommunications Conference (GLOBECOM 2010), 2010 IEEE*, pages 1–5. IEEE, 2010.